# Computational Assessment of Microrotation and Buoyancy Effects on the Stagnation Point Flow of Carreau–Yasuda Hybrid Nanofluid with Chemical Reaction Past a Convectively Heated Riga Plate

Muhammad Ramzan, Muhammad Javed, Sadique Rehman, Dawood Ahmed, Anwar Saeed,* and Poom Kumam*

ACCESS | Metrics & More | Article Recommendations

**ABSTRACT:** The present framework deliberated the mixed convection stagnation point flow of a micropolar Carreau–Yasuda hybrid nanoliquid through the influence of the Darcy-Forchheimer parameter in porous media toward a convectively heated Riga plate. In this investigation, blood is used as a base liquid and gold (Au) and copper (Cu) are the nanoparticles. The main novelty of the present investigation is to discuss the transmission of heat through the application of thermal radiation, viscous dissipation, and the heat source/sink on the flow of a micropolar Carreau–Yasuda hybrid nanoliquid. Further, the results of the chemical reaction are utilized for the computation of mass transport. Brownian motion and thermophoretic phenomena are discussed in the current investigation. The current problem is evaluated by using the connective and partial slip conditions and is formulated on the basis of the higher-order nonlinear PDEs



which are converted into highly nonlinear ODEs by exploiting the similarity replacement. In the methodology section, the homotopic analysis scheme is employed on these resulting ODEs for the analytical solution. In the discussion section, the results of the different flow parameters on the velocity, microrotation, energy, and mass of the hybrid nanofluid are computed against various flow parameters in a graphical form. Some of the main conclusions related to the present investigation are that the velocity profile is lowered but the temperature is augmented for both nanoparticles volume fractions. It is notable that the skin friction coefficient is reduced due to the higher values of the Darcy-Forchheimer parameter. Further, the rising performance of the hybrid nanofluid Nusselt number is determined by the radiation parameter.
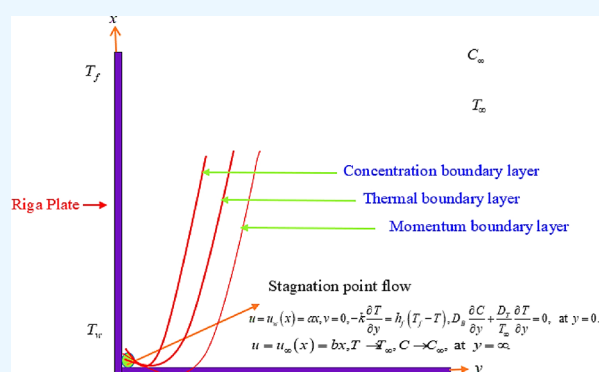
## 1. INTRODUCTION

In the past few years, researchers and scientists have been interested in studying non-Newtonian fluid flow problems due to the extensive variety of applications in different fields of industry and manufacturing. Applications of non-Newtonian fluid flow are oil recovery, food dispensation, movements of the biological fluids, clay mixtures, cosmetics, paper production, pharmaceuticals, nuclear and chemical industries, paints, molten polymers, geophysics, bioengineering, oil storage engineering, paper manufacturing, and many others. Mohamed et al.[1] used parallel plates for the analysis of non-Newtonian nanoliquid flow with the application of the Hall current through the porous media. In this work, it was shown that the energy profile of the nanofluid is increased with the increase of the heat source/sink, but it has the opposite behavior for the Prandtl number. Xia Li et al.[2] utilized the Prandtl and Cattaneo-Christov effective approach to study the periodic flow of the non-Newtonian Casson nanofluid with Darcy-Forchheimer and motile gyrotactic microorganism. From this analysis, it was detected that the

nanofluid velocity declined due to the Casson liquid constant and inertial coefficient. Imtiaz et al.[3] addressed the non-Newtonian Jeffrey liquid flow under the curved stretched surface with the assistance of autocatalytic chemical reactions. They noted that the fluid concentration is enhanced due to the enhancement of the heterogeneous reaction. Gowda et al.[4] exploited the RK-45 scheme for the numerical estimation of the non-Newtonian nanoliquid flow with activation energy. It was detected that the heat transportation is enhanced due to the result of the porosity factor. Ramzan et al.[5] explored the non-Newtonian nanoliquid flow toward the thin needle with entropic

and dipole characteristics with the implementation of the homotopic analysis technique. They proved that the nanoliquid entropic behavior is augmented with the enrichment of the Lewis and Eckert numbers. Soomro et al.[6] reviewed the non-Newtonian nanoliquid flow through the inclusion of thermophoretic and Brownian motion over the vertical stretched surface. They solved their problem numerically by exploiting the finite-difference Crank Nicolson scheme. Bilal and Urwa[7] explained the non-Newtonian liquid flow problem over the thin needle, and this model was evaluated under the prevalence of variable viscosity and activation energy. When they enhanced the value of the buoyancy ratio parameters the drag force increased. Prasannakumara[8] addressed the phenomena of heat transport over the non-Newtonian Maxwell nanoliquid flow by using a stretchy surface. With the use of this model, he showed good thermal performance for a Newtonian fluid as compared to a Maxwell liquid when he increased the ferromagnetic interaction and volume fraction parameters. Further, the flow problems related to the non-Newtonian fluids are studied and discussed in refs 9−11.

Nanofluids play a significant role in the improvement of heat transportation of the base liquid. Because the nanoliquid is created by mixing nanoparticles with the base liquid, it has the power to improve the base fluid's thermal performance. Nanofluid flow has an enormous variety of applications in various arenas of bioscience and engineering including geothermal power extraction, lubricants, cooling of motor vehicles, magnetic resonance imaging (MRI), purification of the biomolecules, and cooling of electronic devices and heat exchangers, nuclear reactor vehicles cooling, thermal management, and many others. Many scientists and researchers have expanded nanofluid research due to its numerous functions. Eswaramoorthi et al.[12] dissected the outcomes of nonlinear thermal radiation over magnetohydrodynamic (MHD) Cu−Ag/water-based nanoliquid flow under a heated plate with the inclusion of a heat transport mechanism and explained that the Nusselt number in Ag-nanoparticles is greater as compared to the Nusselt number in Cu-nanoparticles. Alshehri and Shah[13] discussed the hybrid nanoliquid flow toward an extending surface with the application of viscous dissipation and the Darcy-Forchheimer model. In this investigation, it was noted that the porosity of the fluid decreased the speed of the liquid particles. Waqas et al.[14] inspected the impacts of the motile microorganisms on the 3D Carreau−nanoliquid flow using the bvp4c-technique. Muhammad et al.[15] discovered the effects of the chemical reaction on the bioconvection three-dimensional Jeffrey nanofluid flow by using the stretching surface technique. They determined that the nanoliquid mass contour is decayed for the chemical reaction parameter. Nadeem et al.[16] used convective conditions to discuss the MHD Walter-B nanoliquid flow with Brownian and thermophoresis effects. Ramzan et al.[17] assessed the Burger nanoliquid flow by using a homotopic analysis scheme under a stretching cylinder and sheet and discussed that the escalating estimates of the thermal Biot number rise faster than the Burger nanoliquid Nusselt number. Bilal et al.[18] dissected the energy transport phenomenon over the mixed convection nanofluid flow with a magnetic field toward a revolving disk. Akbar et al.[19] elucidated the role of the Hall effect over the MHD Carreau−Yasuda nanoliquid flow surrounded by a channel through the porous media. From their concluding remarks, it can be determined that the mass rate transport is lower due to the enhancement of the Schmidt number. Li et al.[20] demonstrated the two-phase flow of a non-

Newtonian nanoliquid through a permeable H-shaped cavity with mixed convection surrounded by a porous media. In this model, they also used four rotatable cylinders inside the enclosure. In this work, it is noted that the drag force is augmented with increasing Darcy number. Kavusi and Toghraie[21] numerically analyzed heat pipe performance under the applications of the two-dimensional nanofluid model with the help of the finite volume technique and found that the fluid pressure is enhanced with the enhancement of the thermal capacity of the fluid. Moraveji and Toghrai[22] computationally discussed the energy allocation rate and nanofluid flow features by using the different parameters of a vortex tube. In this article, it was seen that the mass transition rate is enhanced from the cold and hot cross-section area due to the increase in the length of the vortex tube. Ruhani et al.[23] explored statistically the rheological impact of the silica-ethylene glycol-nanoparticles on hybrid ferrofluid flow by manipulating the experimental data with a water-base fluid. In this problem, the fluid is Newtonian due to the linear relationship between shear stress and shear rate. Mostafazadeh et al.[24] scrutinized the consequence of laminar flow of a nanoliquid through a vertical channel with the use of single-and two-phase approaches and deliberated that the kinetic energy for the velocity field is enhanced due to the increment of the fluid temperature. Arasteh et al.[25] considered the role of local nonequilibrium conditions and the Darcy-Forchheimer model on the nanofluid flow. The strong numerical method recognized as the finite volume method was employed for the solution of their problem. More studies on the nanofluid flow problem can be found in refs 26−28.

Hybrid nanofluids are very useful in transmitter and biotechnology, ships, radioactive systems, electrical coolers, generators, automobile industry, air conditioners, heat converters, heat pumps, and solar energy, etc. Hybrid nanofluids provide a more satisfying outcome with respect to heat transport relative to nanoliquids and conventional liquids. As a result, scientists and researchers are very interested in exploring hybrid nanofluid flow difficulties. Xia et al.[29] determined the significance of the Joule heating effect on hybrid nanoliquid flow with entropy optimized dissipative. Here temperature graph is enlarged for the greater estimates of the radiation and magnetic parameters. Kumar et al.[30] deliberated the upshot of the nonuniform heat generation on the dusty hybrid nanoliquid flow toward the rotating disk through the porous media. Jamshed et al.[31] interpreted the Williamson hybrid nanoliquid flow with an engine oil-based liquid by employing the Cattaneo-Christov heat flux model. Anuar and Bachok[32] highlighted the unsteady micropolar hybrid nanoliquid flow at a stagnation point under the occurrence of thermal radiation. They attained numerical solutions to their problem. In this research work, it was distinguished that the hybrid nanoliquid flow is augmented for the higher estimation of the material parameter and unsteady parameter. Mabood et al.[33] documented the convective flow of a hybrid ferrofluid under a stretched sheet. In this problem, the consequence of nonlinear radiation and the irreversible evaluation of the hybrid nanoliquid are also computed. They observed that increasing the estimation of the Bejan number amplified the generation of the liquid entropy. Gowda et al.[34] demonstrated hybrid nanoliquid flow across an enlarging cylinder. In this investigation, it was detected that the fluid particles speed is decreased when the nanoparticulate quantity is enhanced. Haider et al.[35] calculated the occurrence of the Darcy-Forchheimer flow through an absorbent space. They noticed that the hybrid nanoliquid has a lower heat transport proportion
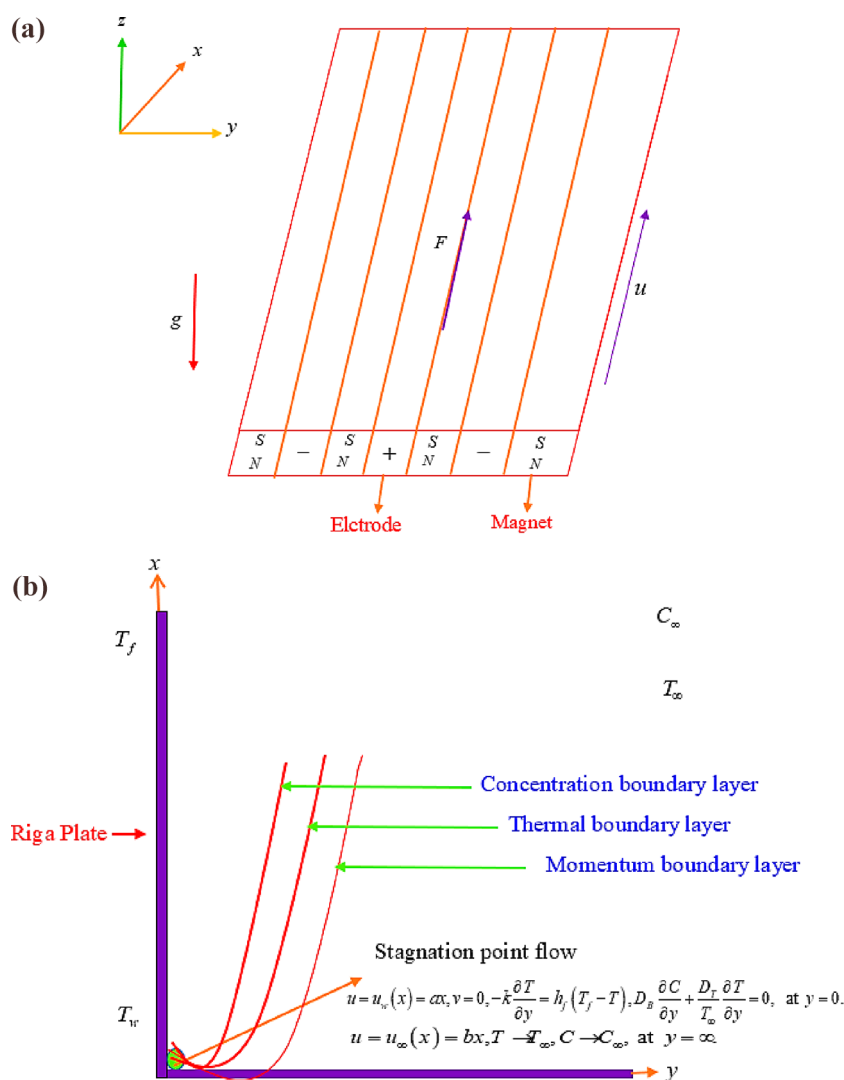
**Figure 1.** (a) Physical view of the Riga plate. (b) Schematic illustration of the problem.

as compared to the titanium dioxide nanoliquid. Ramzan et al.[36] presented the analytical solution of the MHD flow of mixed convection hybrid nanoliquid with slip conditions over a stretchable sheet. In this evaluation, they found that the escalating estimates of the suction parameter decrease the hybrid nanofluid temperature.

Chemical reactions have a variety of engineering and industrial applications. The crop damage owing to the freezing atmosphere, formation of the fog, polymers production, water emulsions, oil, dehydration processes, hydro-metallurgical industries, ceramics, food processing, and manufacturing of papers are some of the industrial and engineering applications of chemical reactions. Many researchers analyze the characteristics of chemical reactions after being inspired by their applicability. Khan et al.[37] evaluated analytically the flow of a micropolar nanoliquid through the impact of viscous dissipation with convective conditions over a rotating thin needle. In this observation, it was perceived that the rising estimates of the chemical reaction parameter decreased the mass allocation. Reddy and Lakshminarayana[38] studied the chemical reaction of the MHD three-dimensional Maxwell nanoliquid flow in the prevalence of an energy source and cross-diffusion under a stretchable sheet. Kumar et al.[39] described the result of the chemical reaction over the Casson nanoliquid flow by using a curved elongating sheet. In this inquiry, it was seen that the streamflow of the nanofluid decreases when the Casson fluid parameter is augmented. Gul et al.[40] explained the magneto-hydrodynamic hybrid nanoliquid flow by using the behavior of the chemical reaction over a stretchable cylinder. Further, they noticed that the expanding estimates of the energy sink parameter increased the energy of the hybrid nanoliquid. Gopal et al.[41] established numerically the model of MHD nanoliquid flow with the manifestation of buoyancy forces through the porous media along a stretched sheet. In this article, it was predicted that the mass transport of the hybrid nanoliquid is decreased due to the intensifying chemical reaction effect. Lv et al.[42] described the consequence of the Hall effect over the nanoliquid flow as a result of a radiation effect through a rotating channel. They discussed that the energy frequency transport is higher for larger evaluations of the Prandtl number. Gowda et al.[43] described the second-grade nanoliquid flow with the existence of the chemical reaction and Brownian diffusivity. In this problem, they found that the augmented approximation of the porosity term decreased the nanoliquid Nusselt number. Rasheed et al.[44] used the convective conditions and internal heating source for the flow of a nanoliquid. It was seen that the expansion in the magnetic parameter led to improving the thermal profile of the nanoliquid.

In the light of the above-cited literature, the current problem is framed for the evaluation of the heat and mass transport phenomena on the mixed convection flow of Carreau–Yasuda hybrid nanofluid toward the convectively heated Riga plate through the porous medium. The hybrid nanofluid is formed by mixing the gold (Au) and copper (Cu) nanoparticulates in the blood-base liquid. The roles of the Darcy-Forchheimer flow, viscous dissipation, chemical reaction, and thermal radiation are computed in the present scrutiny. The micropolar Carreau–Yasuda hybrid nanofluid is the non-Newtonian fluid. So, the daily life examples of such fluids are corn starch, silly putty, some brakes pads in cars, quicksand, and corn flour, etc. A simulation of the higher-order ODEs is performed with the implementation of the homotopic analysis scheme. Effects of the several flow constraints over the velocity, microrotation, mass, and energy of the hybrid nanofluid are computed and discoursed in a graphical form. The Nusselt number and skin friction are scrutinized in contour graphs against numerous flow parameters. At the end of the present investigation, we will be able to find out the answers to the following questions:

- How do the gold and copper nanoparticles affect the mixed convection micropolar Carreau–Yasuda hybrid nanofluid?
- How does the Lorentz force affect the velocity of the micropolar Carreau–Yasuda hybrid nanoliquid by using the Hartmann number?
- What is the behavior of the velocity of the micropolar Carreau–Yasuda hybrid nanofluid versus different flow parameters?
- How does the microrotation profile of the micropolar Carreau–Yasuda hybrid nanofluid behave against the microrotation parameter and microrotation slip parameter?
- What is the behavior of the micropolar Carreau–Yasuda hybrid nanofluid temperature via discrete flow parameters?
- What is the role of the radiation parameter on the Nusselt number?
- How does the skin friction coefficient behave against the Darcy-Forchheimer parameter?

## 2. PROBLEM FORMULATION

Consider the 2D, incompressible and steady flow of a mixed convection micropolar Carreau–Yasuda hybrid nanofluid along with Darcy-Forchheimer behavior in a porous medium under the convectively heated Riga plate. Also, assume that the fluid is pseudoplastic. In this study, blood is used as a base liquid and gold (Au) and copper (Cu) are used as the nanomaterials. By combining the electrodes and magnets the Riga plate is designed for the present problem. Effects of thermal radiations, heat source, and viscous dissipations are employed for the evaluation of heat transport under convective and partial slip conditions. Additionally, the roles of Brownian motion and thermophoretic are evaluated. The phenomena of mass transport are considered by using the chemical reaction. The velocity of the stretching sheet is $u_w(x) = ax$ and the ambient velocity of the liquid is $u_\infty(x) = bx$, but the origin is fixed. Here $T_f$ is the convective liquid temperature but the ambient temperature of the liquid is $T_\infty$. For the formulation of the current problem, the $x$-axis is taken upright while the $y$-axis is horizontal over the Riga plate in the Cartesian coordinate system. Figure 1 panels a and b are designed for the physical illustration of the current model.

The equation for a Carreau–Yasuda fluid is[45]

$$\tau = [\mu_\infty + (\mu_0 - \mu_\infty)((1 + \Gamma\dot\gamma)^d)^{((n-1)/d)}]A_1 \tag{1}$$

Here $\mu_0$ and $\mu_\infty$ are the zero and infinite shear rate viscosity. The parameters for the Carreau–Yasuda liquid are $\Gamma$ and $d$. $A_1$ is the Rivlin-Ericksen tensor and $\tau$ is the extra stress tensor, $\dot\gamma$ is $\dot\gamma = \sqrt{tr(A_1^2)\left(\frac{1}{2}\right)}$ and $A_1 = [(gradv)^t + gradv]$. When $\mu_\infty = 0$ eq 1 becomes

$$\tau = [\mu_0((1 + \Gamma\dot\gamma)^d)^{((n-1)/d)}]A_1 \tag{2}$$

By considering the above-mentioned assumptions on the flow behavior, the governing equations of the presented model are[45−48]

$$\frac{\partial u}{\partial x} + \frac{\partial v}{\partial y} = 0 \tag{3}$$

$$u\frac{\partial u}{\partial x} + v\frac{\partial u}{\partial y} = u_\infty\frac{du_\infty}{dx} + \left(\frac{\mu_{hnf} + k_1^*}{\rho_{hnf}}\right)\frac{\partial^2 u}{\partial y^2} + \left(\frac{k_1^*}{\rho_{hnf}}\right)\frac{\partial N^*}{\partial y}$$
$$+ \nu_{hnf}\left(\frac{(n-1)}{d}(d+1)\Gamma^d\left(\frac{\partial u}{\partial y}\right)^d\frac{\partial^2 u}{\partial y^2}\right)$$
$$+ g\left(\frac{(1-C)\beta\rho_{fm}}{\rho_f}(T - T_\infty) - \left(\frac{\rho_p - \rho_{fm}}{\rho_p}\right)(C - C_\infty)\right)$$
$$+ \frac{\pi j_0 M_0}{8\rho_f}e^{-(\frac{\pi}{a_1})y} - \frac{\nu_{hnf}}{k_p}u - Fu^2 \tag{4}$$

$$u\frac{\partial N^*}{\partial x} + v\frac{\partial N^*}{\partial y} = \frac{\gamma_{hnf}^*}{j^*\rho_{hnf}}\frac{\partial^2 N^*}{\partial y^2} - \frac{k_1^*}{j^*\rho_{hnf}}\left(2N^* + \frac{\partial u}{\partial y}\right) \tag{5}$$

$$u\frac{\partial T}{\partial x} + v\frac{\partial T}{\partial y} = \left(\frac{k_{hnf}}{(\rho C_p)_{hnf}} + \frac{16\sigma^* T_\infty^3}{3k^*(\rho C_p)_{hnf}}\right)\frac{\partial^2 T}{\partial y^2}$$
$$+ \tau\left(D_B\frac{\partial C}{\partial y}\frac{\partial T}{\partial y} + \left(\frac{\partial T}{\partial y}\right)^2\left(\frac{D_T}{T_\infty}\right)\right) + \frac{\mu_{hnf}}{(\rho C_p)_{hnf}}\left(\frac{\partial u}{\partial y}\right)^2$$
$$+ \frac{Q_0}{(\rho C_p)_{hnf}}(T - T_\infty) \tag{6}$$

$$u\frac{\partial C}{\partial x} + v\frac{\partial C}{\partial y} = D_B\frac{\partial^2 C}{\partial y^2} + \left(\frac{D_T}{T_\infty}\right)\frac{\partial^2 T}{\partial y^2}, -k_r^2(C - C_\infty) \tag{7}$$

The components of velocity along the directions of $x$-axis and $y$-axis are $u$ and $v$. The ambient velocity is $u_\infty$, the hybrid nanofluid dynamics viscosity is $\mu_{hnf}$, the vortex viscosity is $k_1^*$, $N^*$ is the microrotation parameter, the hybrid nanoliquid viscosity is $\nu_{hnf}$, $n$ is the power index, the parameters for the Carreau–Yasuda hybrid nanoliquid are $\Gamma$ and $d$, the gravitational acceleration is $g$, $C_\infty$ is the ambient concentration of the liquid, $\beta$ is the thermal expansion factor, $j_0$ is the current density, the magnetization of the magnet is $M_0$, $\rho_f$ is the base liquid density, $\rho_p$ is the density of the particles, $T$ and $T_\infty$ are the temperature and ambient temperature of the liquid correspondingly, the inertia is $F = \frac{C_b}{\sqrt{k_c}}$

in which the drag coefficient is $C_b$, $\gamma_{hnf}^* = \left(\mu_{hnf} + \frac{k_1^*}{2}\right)j^*$ is the spin gradient, where the length scale parameter is expressed by $j^* = \frac{\nu}{a}$, the thermal conductivity of the hybrid nanoliquid is $k_{hnf}$, at a constant pressure the specific heat is $C_p$, $\sigma^*$ is the Stefan–Boltzmann constant and the coefficient of absorption is $k^*$, $\tau$ is the ratio between the nanoparticles heat capacity and base liquid capacity, $D_B$ and $D_T$ are the Brownian and thermal diffusion factors, $Q_0$ is the heat source/sink, and $k_r^2$ is the chemical reaction rate constant.

The boundary conditions

$$\left\{\begin{array}{l} u = u_w(x) = ax, \quad v = 0, \quad N^* = -m_0\dfrac{\partial u}{\partial y}, \\[2mm] -k_{hnf}\dfrac{\partial T}{\partial y} = h_f(T_f - T), \quad D_B\dfrac{\partial C}{\partial y} + \dfrac{\partial T}{\partial y}\dfrac{D_T}{T_\infty} = 0, \quad \text{at } y = 0, \\[2mm] u = u_\infty(x) = bx, \quad N^* \to 0, \quad T \to T_\infty, \quad C \to C_\infty, \quad \text{at } y = \infty \end{array}\right. \tag{8}$$

In the above-mentioned boundary conditions, $u_w$ is the velocity of the stretching surface, $a$ and $b$ are constants, $N^*$ is the microrotation parameter, the microrotation slip parameter is $m_0$, the thermal conductivity is $k$, and the ambient velocity is $u_\infty$.

The thermophysical properties of the hybrid nanofluid are defined as

$$\left\{\begin{array}{l} \dfrac{k_{hnf}}{k_f} = \dfrac{\left(\dfrac{\phi_1 k s_1 + \phi_2 k s_2}{\phi_{hnf}}\right) + 2k_f + 2(\phi_1 k s_1 + \phi_2 k s_2) - 2\phi_{hnf}k_f}{\left(\dfrac{\phi_1 k s_1 + \phi_2 \rho s_2}{\phi_{hnf}}\right) + 2k_f - (\phi_1 k s_1 + \phi_2 k s_2) + \phi_{hnf}k_f}, \\[4mm] \rho_{hnf} = (1 - \phi_{hnf})\rho_f + \phi_2 \rho s_2 + \phi_1 \rho s_1, \phi_{hnf} = (\phi_1 + \phi_2), \mu_{hnf} \\[2mm] \quad = \dfrac{\mu_f}{(1 - \phi_{hnf})^{2.5}}, \\[3mm] (\rho C_p)_{hnf} = (1 - \phi_{hnf})(\rho C_p)_f + (\rho C_p)_{s1}\phi_1 + (\rho C_p)_{s2}\phi_2, \\[3mm] \dfrac{\sigma_{hnf}}{\sigma_f} = \dfrac{\left(\dfrac{\phi_1 \rho s_1 + \phi_2 \rho s_2}{\phi_{hnf}}\right) + 2\sigma_f + 2(\phi_1 \rho s_1 + \phi_2 \rho s_2) - 2\phi_{hnf}\sigma_f}{\left(\dfrac{\phi_1 \rho s_1 + \phi_2 \rho s_2}{\phi_{hnf}}\right) + 2\sigma_f - (\phi_1 \rho s_1 + \phi_2 \rho s_2) + \phi_{hnf}\sigma_f}, \end{array}\right. \tag{9}$$

Here hybrid nanoliquid thermal conductivity is $k_{hnf}$, the base liquid thermal conductivity is $k_f$, $\phi_1$ is the nanoparticle volume fraction of the first nanoparticle, the nanoparticle volume fraction of the second nanoparticle is $\phi_2$, $\rho_{hnf}$ is the hybrid nanofluid density, the base liquid density is $\rho_f$, the density of the first and second nanoparticles is $\rho s_1$ and $\rho s_2$, $\mu_{hnf}$ is the dynamic viscosity of the hybrid nanofluid, $\mu_f$ is the base fluid dynamic viscosity, $(C_p)_{hnf}$ is the specific heat constant of the hybrid nanofluid, the specific heat constant of the base fluid is $(C_p)_f$, $(\rho C_p)_{s1}$ and $(\rho C_p)_{s2}$ are the specific heat constants of the first and second nanoparticles, and $\sigma_f$ is the electrical conductivity of the base fluid.

Table 1 lists the physical properties of the base liquid and nanoparticles.

Similarity transformation is defined as

**Table 1. Thermophysical Characteristics of the Base Liquid and Nanoparticles[49]**

| property | blood | Au (gold) | Cu (copper) |
|---|---|---|---|
| $C_p$ (J/(kg·K)) | 3594 | 129 | 385 |
| $\rho$ (kg/m$^3$) | 1063 | 19320 | 8933 |
| $k$ (W/(m·K)) | 0.492 | 314 | 401 |
| $\beta_T \times 10^{-5}$ (1/K) | 0.18 | 1.4 | 1.67 |
| $\sigma$ (S/m) | $6.67 \times 10^{-1}$ | $4.10 \times 10^7$ | $59.6 \times 10^6$ |

$$\left\{\begin{array}{l} \psi = \sqrt{\alpha\nu_f}\,xf(\zeta), \quad u = \dfrac{\partial\psi}{\partial y} = \alpha x f'(\zeta), \\[3mm] v = -\dfrac{\partial\psi}{\partial x} = -\sqrt{a\nu_f}\,f(\zeta), \quad N^* = ax\sqrt{\dfrac{a}{\nu}}\,G(\zeta), \\[3mm] \theta(\zeta) = \dfrac{T - T_\infty}{T_f - T_\infty}, \\[3mm] \phi(\zeta) = \dfrac{C - C_\infty}{C_\infty}, \quad \zeta = \sqrt{\dfrac{a}{\nu_f}}\,y \end{array}\right. \tag{10}$$

By using the above similarity variables defined in Eq. 10, it is obtained that

$$\begin{aligned} &\left(\left(\dfrac{\mu_{hnf}}{\rho_{hnf}}\right)f''' + A_3\left(\dfrac{\rho_f}{\rho_{hnf}}\right)(A_1 + K)f''' \right. \\ &\left. + \left(\dfrac{\mu_{hnf}}{\rho_{hnf}}\right)\dfrac{(n-1)}{d}(d+1)W_e^d(f'')^d f''' \right) + r^2 + ff'' \\ &- (1 + Fr)(f')^2 - \lambda_1 f' + KG' + \lambda\theta - Nr\phi \\ &+ Hae^{-\gamma\eta} = 0 \end{aligned} \tag{11}$$

$$\left(\dfrac{\mu_{hnf}}{\mu_f} + \dfrac{K}{2}\right)G'' + fG' - f'G - \left(\dfrac{\rho_f}{\rho_{hnf}}\right)K(2G - f'') = 0 \tag{12}$$

$$\begin{aligned} &\left(1 + \dfrac{4}{3}R\right)\theta'' + \Pr\dfrac{(\rho C_p)_{hnf}/(\rho C_p)_f}{(k_{hnf}/k_f)}(Nb\theta'\phi' + f\theta') \\ &+ Nt(\theta')^2 + Q\theta + \dfrac{(\mu_{hnf}/\mu_f)}{((\rho C_p)_{hnf}/(\rho C_p)_f)}Ec(f'')^2 = 0 \end{aligned} \tag{13}$$

$$\phi'' + Sc\phi' - krSc\phi + \dfrac{Nt}{Nb}\theta'' = 0 \tag{14}$$

and the converted boundary conditions are

$$\left\{\begin{array}{l} f = 0, \quad f' = 1, \quad G = -m_0 f'', \\[2mm] k_{hnf}\theta' = -Bi(1 - \theta), \quad Nt\theta' + Nb\phi' = 0 \\[2mm] \text{at } \eta \to 0, \\[2mm] f' = r, \quad G \to 0, \quad \theta \to 0, \quad \phi \to 0 \quad \text{at } \eta \to \infty, \end{array}\right. \tag{15}$$

After the simplification of the present problem some important nondimensional parameters are listed here:

Weissenberg number:

$$We = \frac{a^{3/2}x\Gamma}{\sqrt{\nu_f}}$$

Stretching parameter:

$$r = \frac{b}{a}$$

Darcy-Forchheimer parameter:

$$Fr = \frac{C_b x}{\sqrt{k_c}}$$

Buoyancy ratio parameter:

$$Nr = \frac{(\rho_p - \rho_{fm})C_\infty g}{a^2 x \rho_f}$$

Mixed convection parameter:

$$\lambda = \frac{(1 - C)\beta\rho_{fm}(T_f - T_\infty)g}{a^2 x \rho_f}$$

Hartmann number:

$$Ha = \frac{\pi j_0 M_0 x}{8\rho_p u_w^2}$$

Width parameter:

$$\gamma = \frac{-\pi}{a_1\sqrt{\left(\frac{a}{\nu_f}\right)}}$$

Thermal radiation:

$$R = \frac{4\sigma^* T_\infty^3}{k_f k^*}$$

Heat generation parameter:

$$Q = \frac{Q_0}{a(\rho C_p)_f}$$

Brownian motion parameter:

$$Nb = \frac{\tau D_B C_\infty}{\nu_f}$$

Thermophoresis:

$$Nt = \frac{\tau D_T (T_f - T_\infty)}{\nu_f T_\infty}$$

Eckert number:

$$Ec = \frac{u_w^2}{(\rho C_p)_f(T_f - T_\infty)}$$

Schmidt number:

$$Sc = \frac{\nu_f}{D_B}$$

Chemical reaction constraint:

$$kr = \frac{k_r^2}{a}$$

Microrotation parameter:

$$K = \frac{K_1^*}{\mu_f}$$

Prandtl number:

$$\Pr = \frac{\nu_f (\rho C_p)_f}{k_f}$$

Porosity parameter:

$$\lambda_1 = \frac{\nu_f}{k_p a}$$

In the current examination the physical quantities are discussed as

$$\begin{cases} Cf = \dfrac{\tau_w}{\rho_{hnf} u_w^2}, \\[2ex] Nu_x = \dfrac{x q_w}{k_f(T_f - T_\infty)} \end{cases} \tag{16}$$

with $\tau_w$ and $q_w$

$$\begin{cases} \tau_w = \mu_{hnf}\left\{\left(1 + \dfrac{K}{2}\right)\left(1 + \left(\dfrac{n-1}{d}\right)\Gamma^d\left(\dfrac{\partial u}{\partial y}\right)^d\right)\dfrac{\partial u}{\partial y}\right\}\Bigg|_{y=0}, \\[3ex] q_w = -\left(\dfrac{k_{hnf}}{k_f} + \dfrac{4}{3}R\right)\left(\dfrac{\partial T}{\partial y}\right)_{y=0} \end{cases} \tag{17}$$

After the simplification, the dimensionless form of eq 16 is

$$\begin{cases} Cf Re_x^{1/2} = \dfrac{\mu_{hnf}}{\mu_f}\left(1 + \dfrac{K}{2}\right)\left(1 + \left(\dfrac{n-1}{2}\right)We^d f''^d\right)f'', \\[3ex] Nu_x Re_x^{-1/2} = -\left(\dfrac{k_{hnf}}{k_f} + \dfrac{4}{3}R\right)\theta'(0) \end{cases} \tag{18}$$

$Re_x = \frac{u_w x}{\nu_f}$ is the Reynolds number.

## 3. SOLUTION OF THE PROBLEM

In the physical situation, sometimes the mathematically modeled problem is not solved easily especially in the case of highly nonlinear differential equations. For the solution of such a nonlinear system of equations, the scientists and mathematicians have developed a different type of techniques. By using the HAM technique,[50−55] the various physical models related to fluid mechanics have been studied by different researchers. The advantage of the homotopy analysis method over the other methods are as follows:

- Homotopy analysis method is a generalized method because it is valid for both strongly and weakly nonlinear problems.

- This scheme is independent of small and large constraints.

- Any sort of nonlinear PDEs without discretization and linearization can be solved by using this technique.

- This method is linear and does not require any base function.

- Series and convergent solutions of the system are determined by using this method.

The present problem is simulated by using the HAM scheme. For this, the initial guess is determined as

$$
\begin{cases}
f_0(\zeta) = r\zeta + (1 - r)(1 - e^{-\zeta}), \\
G_0 = m_0(1 - r)\, e^{-\zeta}\; \theta_0(\zeta) = \dfrac{B_i}{1 + B_i}\, e^{-\zeta}, \\
\phi_0(\xi) = -\dfrac{Nt}{Nb}\dfrac{B_i}{(1 + B_i)}\, e^{-\zeta}
\end{cases}
\tag{19}
$$

and the linear operators are

$$
\mathbf{L}_f(\zeta) = f''' - f', \qquad \mathbf{L}_G(\zeta) = G'' - G,
$$
$$
\mathbf{L}_\theta(\zeta) = \theta'' - \theta, \qquad \mathbf{L}_\phi(\zeta) = \phi'' - \phi
\tag{20}
$$

with properties

$$
\begin{cases}
\mathbf{L}_f(J_1 + J_2 \exp(\zeta) + J_3 \exp(-\zeta)) = 0, \\
\mathbf{L}_G(J_4 \exp(\zeta) + J_5 \exp(-\zeta)) = 0, \\
\mathbf{L}_\theta(J_6 \exp(\zeta) + J_7 \exp(-\zeta)) = 0, \\
\mathbf{L}_\phi(J_8 \exp(\zeta) + J_9 \exp(-\zeta)) = 0
\end{cases}
\tag{21}
$$

where $J_i (i = 1, 2, 3, \cdots, 9)$ are the constants.

**3.1. Zeroth Order Deformation Problem.** In the present problem, the zero-order deformations are

$$
(1 - \varepsilon)L_f[f(\zeta, \varepsilon) - f_0(\zeta)]
$$
$$
= qh_f N_f[f(\zeta, \varepsilon), G(\zeta, \varepsilon), \theta(\zeta, \varepsilon), \phi(\zeta, \varepsilon)]
\tag{22}
$$

$$
(1 - \varepsilon)L_G[G(\zeta, \varepsilon) - G_0(\zeta)] = qh_G N_G[f(\zeta, \varepsilon), G(\zeta, \varepsilon)]
\tag{23}
$$

$$
(1 - \varepsilon)L_\theta[\theta(\zeta, \varepsilon) - \theta_0(\zeta)]
$$
$$
= qh_\theta N_\theta[f(\zeta, \varepsilon), \theta(\zeta, \varepsilon), \phi(\zeta, \varepsilon)]
\tag{24}
$$

$$
(1 - \varepsilon)L_\phi[\phi(\zeta, \varepsilon) - \phi_0(\zeta)] = qh_\phi N_\phi[\theta(\zeta, \varepsilon), \phi(\zeta, \varepsilon)]
\tag{25}
$$

Here $\varepsilon$ is the embedding, and $h_f$ $h_G$, $h_\theta$, and $h_\phi$ are the nonzero auxiliary factors. $N_f$ $N_G$, $N_\theta$, and $N_\varphi$ are the nonlinear operator and discoursed as

$$
N_f[f(\zeta, \varepsilon), G(\zeta, \varepsilon), \theta(\zeta, \varepsilon), \phi(\zeta, \varepsilon)]
$$
$$
= \left(\left(\frac{\mu_{hnf}}{\rho_{hnf}}\right)\frac{\partial^3 f(\zeta, \varepsilon)}{\partial \zeta^3} + A_3\left(\frac{\rho_f}{\rho_{hnf}}\right)(A_1 + K)\frac{\partial^3 f(\zeta, \varepsilon)}{\partial \zeta^3}\right.
$$
$$
+ \left.\left(\frac{\mu_{hnf}}{\rho_{hnf}}\right)\frac{(n - 1)}{d}(d + 1)W_e^d\left(\frac{\partial^2 f(\zeta, \varepsilon)}{\partial \zeta^2}\right)^d\frac{\partial^3 f(\zeta, \varepsilon)}{\partial \zeta^3}\right)
$$
$$
+ r^2 + \frac{\partial f(\zeta, \varepsilon)}{\partial \zeta}\frac{\partial^2 f(\zeta, \varepsilon)}{\partial \zeta^2} - (1 + Fr)\left(\frac{\partial f(\zeta, \varepsilon)}{\partial \zeta}\right)^2
$$
$$
- \lambda_1\frac{\partial f(\zeta, \varepsilon)}{\partial \zeta} + K\frac{\partial G(\zeta, \varepsilon)}{\partial \zeta} + \lambda\theta(\zeta, \varepsilon)
$$
$$
- Nr\phi(\zeta, \varepsilon) + Hae^{-\gamma\eta} = 0
\tag{26}
$$

$$
N_f[f(\zeta, \varepsilon), G(\zeta, \varepsilon)]
$$
$$
= \left(\frac{1}{(1 - \phi_1)^{2.5}(1 - \phi_2)^{2.5}} + \frac{K}{2}\right)\frac{\partial^2 G(\zeta, \varepsilon)}{\partial \zeta^2}
$$
$$
+ f(\zeta, \varepsilon)\frac{\partial G(\zeta, \varepsilon)}{\partial \zeta} - G(\zeta, \varepsilon)\frac{\partial f(\zeta, \varepsilon)}{\partial \zeta}f'G
$$
$$
- \left(\frac{\rho_f}{\rho_{hnf}}\right)K\left(2G(\zeta, \varepsilon) - \frac{\partial^2 f(\zeta, \varepsilon)}{\partial \zeta^2}\right) = 0
\tag{27}
$$

$$
N_\theta[f(\zeta, \varepsilon), \theta(\zeta, \varepsilon), \phi(\zeta, \varepsilon)]
$$
$$
= \left(1 + \frac{4}{3}R\right)\frac{\partial^2 \theta(\zeta, \varepsilon)}{\partial \zeta^2} + \Pr\frac{(\rho C_p)_{hnf}/(\rho C_p)_f}{(k_{hnf}/k_f)}
$$
$$
\left(Nb\frac{\partial \theta(\zeta, \varepsilon)}{\partial \zeta}\frac{\partial \phi(\zeta, \varepsilon)}{\partial \zeta} + f(\zeta, \varepsilon)\frac{\partial \theta(\zeta, \varepsilon)}{\partial \zeta}\right.
$$
$$
+ Nt\left(\frac{\partial \theta(\zeta, \varepsilon)}{\partial \zeta}\right)^2 + \left.Q\theta(\zeta, \varepsilon)\right)
$$
$$
+ \frac{(\mu_{hnf}/\mu_f)}{((\rho C_p)_{hnf}/(\rho C_p)_f)}Ec\left(\frac{\partial^2 f(\zeta, \varepsilon)}{\partial \zeta^2}\right)^2
\tag{28}
$$

$$
N_\phi[\theta(\zeta, \varepsilon), \phi(\zeta, \varepsilon)] = \frac{\partial^2 \phi(\zeta, \varepsilon)}{\partial \zeta^2}\phi'' + Sc\frac{\partial \phi(\zeta, \varepsilon)}{\partial \zeta}
$$
$$
- krSc\phi(\zeta, \varepsilon) + \frac{Nt}{Nb}\frac{\partial^2 \theta(\zeta, \varepsilon)}{\partial \zeta^2}
\tag{29}
$$

$$
f(0, \varepsilon) = 0, \quad f'(0, \varepsilon) = 1, \quad \text{and} f'(\infty, \varepsilon) = r
\tag{30}
$$

$$
G(0, \varepsilon) = -m_0 f''(0, \varepsilon) \quad \text{and} \quad G(\infty, l) = 0
\tag{31}
$$

$$
k_{hnf}\theta'(0, \varepsilon) = -B_i(1 - \theta(0, \varepsilon)) \quad \text{and} \quad \theta(\infty, \varepsilon) = 0
\tag{32}
$$

$$
Nt\theta'(0, \varepsilon) + Nb\phi'(0, \varepsilon) = 0 \quad \text{and} \quad \phi(\infty, \varepsilon) = 0
\tag{33}
$$

For $\varepsilon = 0$ and $\varepsilon = 1$ eqs 22−25 become

$$
\varepsilon = 0 \Rightarrow f(\zeta, 0) = f_0(\zeta) \quad \text{and}
$$
$$
\varepsilon = 1 \Rightarrow f(\zeta, 1) = f(\zeta)
\tag{34}
$$

$$\varepsilon = 0 \Rightarrow G(\zeta, 0) = G_0(\zeta) \quad \text{and}$$
$$\varepsilon = 1 \Rightarrow G(\zeta, 1) = G(\zeta) \tag{35}$$

$$\varepsilon = 0 \Rightarrow \theta(\zeta, 0) = \theta_0(\zeta) \quad \text{and}$$
$$\varepsilon = 1 \Rightarrow \theta(\zeta, 1) = \theta(\zeta) \tag{36}$$

$$\varepsilon = 0 \Rightarrow \phi(\zeta, 0) = \phi_0(\zeta) \quad \text{and}$$
$$\varepsilon = 1 \Rightarrow \phi(\zeta, 1) = \phi(\zeta) \tag{37}$$

The Taylor series expansion is applied to eqs 34−37 and it is obtained that

$$f(\zeta, \varepsilon) = f_0(\zeta) + \sum_{m=1}^{\infty} f_m(\zeta)\varepsilon^m,$$
$$f_m(\zeta) = \frac{1}{m!} \frac{\partial^m f(\zeta, \varepsilon)}{\partial \zeta^m}\big|_{\varepsilon=0} \tag{38}$$

$$G(\zeta, \varepsilon) = G_0(\zeta) + \sum_{m=1}^{\infty} G_m(\zeta)\varepsilon^m,$$
$$G_m(\zeta) = \frac{1}{m!} \frac{\partial^m G(\zeta, \varepsilon)}{\partial \zeta^m}\big|_{\varepsilon=0} \tag{39}$$

$$\theta(\zeta, \varepsilon) = \theta_0(\zeta) + \sum_{m=1}^{\infty} \theta_m(\zeta)\varepsilon^m,$$
$$\theta_m(\zeta) = \frac{1}{m!} \frac{\partial^m \theta(\zeta, \varepsilon)}{\partial \zeta^m}\big|_{\varepsilon=0} \tag{40}$$

$$\phi(\zeta, \varepsilon) = \phi_0(\zeta) + \sum_{m=1}^{\infty} \phi_m(\zeta)\varepsilon^m,$$
$$\phi_m(\zeta) = \frac{1}{m!} \frac{\partial^m \phi(\zeta, \varepsilon)}{\partial \zeta^m}\big|_{\varepsilon=0} \tag{41}$$

By putting $\varepsilon = 1$, in eqs 38−41, the convergence of the series is achieved as

$$f(\zeta) = f_0(\zeta) + \sum_{m=1}^{\infty} f_m(\zeta) \tag{42}$$

$$G(\zeta) = G_0(\zeta) + \sum_{m=1}^{\infty} G_m(\zeta) \tag{43}$$

$$\theta(\zeta) = \theta_0(\zeta) + \sum_{m=1}^{\infty} \theta_m(\zeta) \tag{44}$$

$$\phi(\zeta) = \phi_0(\zeta) + \sum_{m=1}^{\infty} \phi_m(\zeta) \tag{45}$$

**3.2. $m$th Order Deformation Problem.** The $m$th order form of the problem is

$$L_f[f_m(\zeta) - \eta_m f_{m-1}(\zeta)] = h_F R_m^f m(\zeta) \tag{46}$$

$$L_G[G_m(\zeta) - \eta_m G_{m-1}(\zeta)] = h_F R_m^G m(\zeta) \tag{47}$$

$$L_\theta[\theta_m(\zeta) - \eta_m \theta_{m-1}(\zeta)] = h_G R_m^\theta m(\zeta) \tag{48}$$

$$L_\phi[\phi_m(\zeta) - \eta_m \phi_{m-1}(\zeta)] = h_\theta R_m^\phi m(\zeta) \tag{49}$$

$$f_m(0) = 0, \quad f_m(\infty) = 0 \tag{50}$$

$$G_m(0) = 0, \quad G_m(\infty) = 0 \tag{51}$$

$$\theta_m(0) = 0, \quad \theta_m(\infty) = 0 \tag{52}$$

$$\phi_m(0) = 0, \quad \phi_m(\infty) = 0 \tag{53}$$

The $R_m^f m(\zeta)$, $R_m^G m(\zeta)$, $R_m^\theta m(\zeta)$, and $R_m^\phi m(\zeta)$ are defined as

$$R_m^f(\zeta) = \left(\left(\frac{\mu_{hnf}}{\rho_{hnf}}\right) f_{m-1}''' + A_3\left(\frac{\rho_f}{\rho_{hnf}}\right)(A_1 + K)f_{m-1}'''\right.$$
$$+ \left(\frac{\mu_{hnf}}{\rho_{hnf}}\right)\frac{(n-1)}{d}(d+1)W_e^d \sum_{k=0}^{m-1}(f_{m-1-k}'')^d f_k''' + r^2$$
$$+ \sum_{k=0}^{m-1} f_{m-1-k}f_k'' - (1+Fr)\sum_{k=0}^{m-1} f_{m-1-k}'f_k' - f_{m-1}'$$
$$\left. + KG_{m-1}' + \lambda\theta_{m-1} - Nr\phi_{m-1} + Hae^{-\gamma\eta} = 0 \right) \tag{54}$$

$$R_m^G(\zeta) = \left(\frac{\mu_{hnf}}{\mu_f} + \frac{K}{2}\right)G_{m-1}'' + \sum_{k=0}^{m-1} f_{m-1-k}G_k'$$
$$- \sum_{k=0}^{m-1} f_{m-1-k}'G_k - \left(\frac{\rho_f}{\rho_{hnf}}\right)K(2G_{m-1} - f_{m-1}'') = 0 \tag{55}$$

$$R_m^\theta(\zeta) = \left(1 + \frac{4}{3}R\right)\theta_{m-1}'' + Pr\frac{(\rho C_p)_{hnf}/(\rho C_p)_f}{(k_{hnf}/k_f)}$$
$$\left(Nb\sum_{k=0}^{m-1}\theta_{m-1-k}'\phi_k' + \sum_{k=0}^{m-1} f_{m-1-k}\theta_k'\right.$$
$$+ Nt\sum_{k=0}^{m-1}\theta_{m-1-k}'\theta_k' + Q\theta_{m-1}$$
$$\left. + \frac{(\mu_{hnf}/\mu_f)}{((\rho C_p)_{hnf}/(\rho C_p)_f)}Ec\sum_{k=0}^{m-1} f_{m-1-k}''f_k'' = 0\right) \tag{56}$$

$$R_m^\phi(\zeta) = \phi_{m-1}'' + Sc\phi_{m-1}' - krSc\phi_{m-1} + \frac{Nt}{Nb}\theta_{m-1}'' \tag{57}$$

$$\eta_m \begin{cases} 0, & m \le 1 \\ 0, & m > 1 \end{cases} \tag{58}$$

The general solution of the present problem is attained with the use of the particular solution

$$f_m(\zeta) = f_m^*(\zeta) + J_1 + J_2\exp(\zeta) + J_3\exp(-\zeta) \tag{59}$$

$$G_m(\zeta) = G_m^*(\zeta) + J_4\exp(\zeta) + J_5\exp(-\zeta) \tag{60}$$

$$\theta_m(\zeta) = \theta_m^*(\zeta) + J_6\exp(\zeta) + J_7\exp(-\zeta) \tag{61}$$

$$\phi_m(\zeta) = \phi_m^*(\zeta) + J_8\exp(\zeta) + J_9\exp(-\zeta) \tag{62}$$

## 4. RESULTS AND DISCUSSION

The mixed convection stagnation point flow of the micropolar Carreau−Yasuda hybrid nanoliquid toward the convectively heated Riga plate is elaborated. For the analytical explanation of the model the HAM method is used on eqs 11−14 along with boundary conditions eq 15. The physical behavior of the velocity, microrotation, mass, and energy of the hybrid nanofluid are displayed graphically. The computation for the skin friction coefficient and Nusselt number of the hybrid nanoliquid are performed in contour graphs.

**4.1. Velocity Profile.** The influence of the Hartmann number $Ha$, Darcy-Forchheimer factor $Fr$, microrotation parameter $K$, mixed convection parameter $\lambda$, power index number $n$, buoyancy ratio parameter $N_r$, and Weissenberg number $We$ versus velocity contour are observed in Figures 2−10. Figure 2 is captured to evaluate the variation of the hybrid
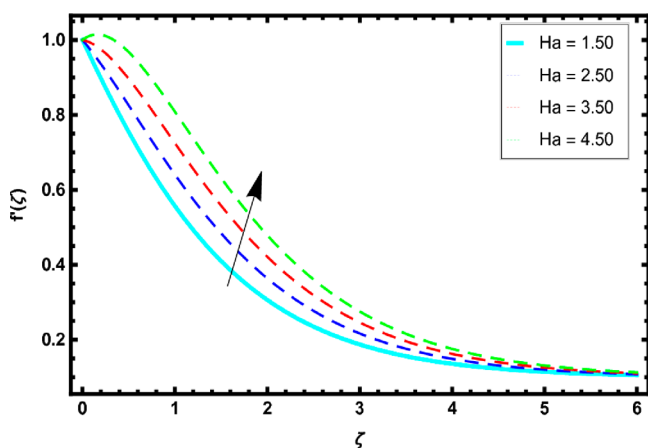


**Figure 2.** Results of velocity outline versus $Ha$.

nanofluid velocity under the effect of the $Ha$. In this figure, it is noticed that the hybrid nanoliquid velocity is amplified when the Hartmann number $Ha$ is enhanced. The external electrical field increases due to the increase of the Hartmann number $Ha$ which consequently increases the hybrid nanoliquid velocity. The boundary layer thickness rises when $Ha$ rises. Also, the Lorentz force is produced when the Hartmann number $Ha$ increases. Figure 3 determines the significance of the Darcy-Forchheimer $Fr$ on hybrid nanofluid velocity. The hybrid nanofluid velocity is
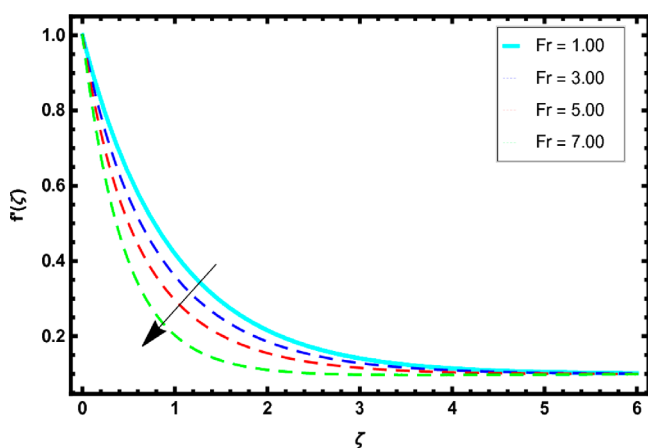


**Figure 3.** Results of velocity outline versus $Fr$.

reduces against the expanding values of the Darcy-Forchheimer parameter $Fr$. The Forchheimer concept is applied for the modeling of the Darcy-Forchheimer parameter, and the $Fr$ has a nonlinear relationship against the flow of the liquid. Further, the thickness of the motion of the fluid particles is enhanced when the $Fr$ is enhanced. When the applications of the Forchheimer theory are discussed then the retardation force is visualized. The liquid motion is slowed due to the upsurge of the porosity of the surface because the $Fr$ is associated with the porosity of the surface. So, the liquid velocity is lower when the Darcy-Forchheimer parameter is higher.

Figure 4 depicts the fluctuation of the velocity outline via discrete values of the microrotation parameter $K$. It is viewed
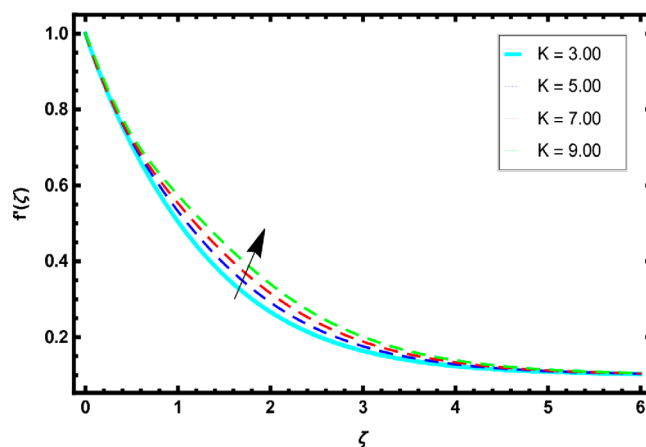


**Figure 4.** Results of velocity outline versus $K$.

that the velocity profile is heightened due to the escalating estimates of the microrotation constant $K$. It is spotted that with the escalation of the microrotation parameter $K$, the boundary layer thickness diminishes. The outcome of $\lambda$ on the velocity profile is debated in Figure 5. In this inquiry, it can be seen that
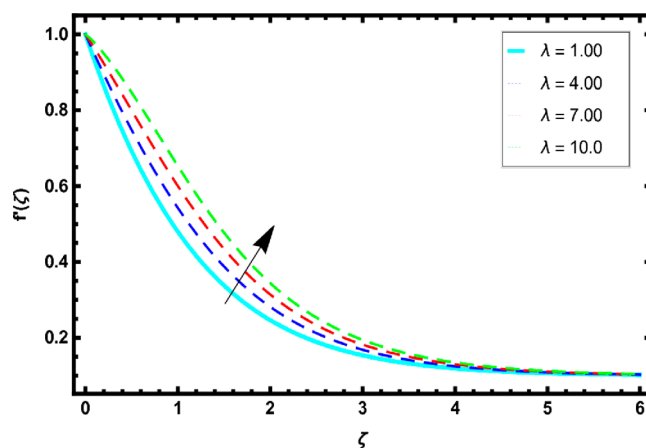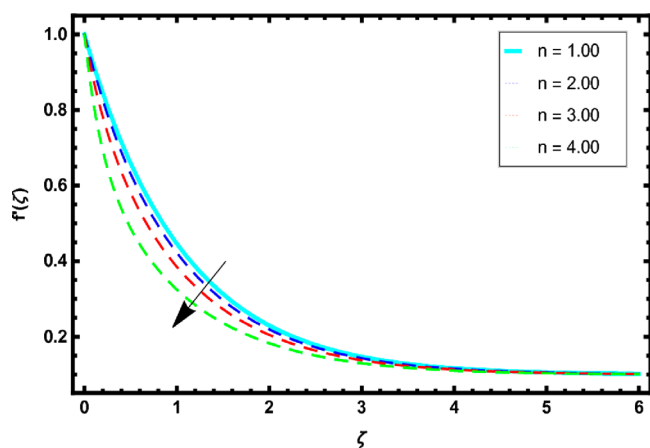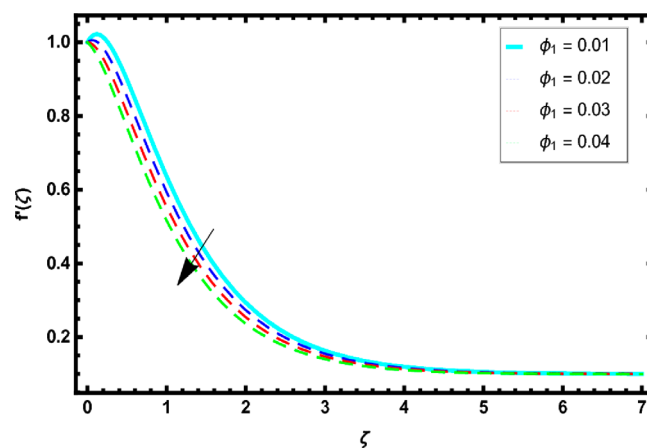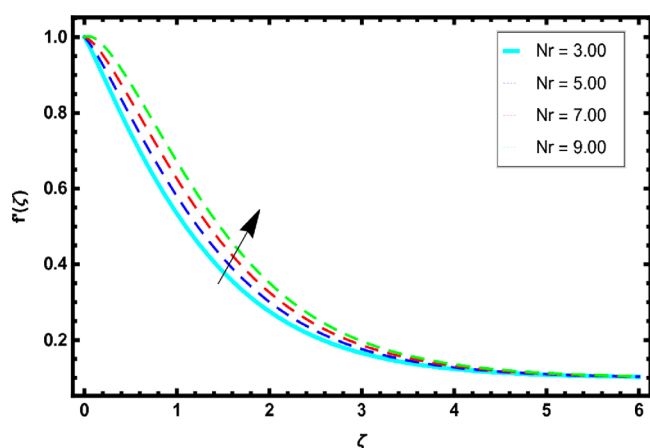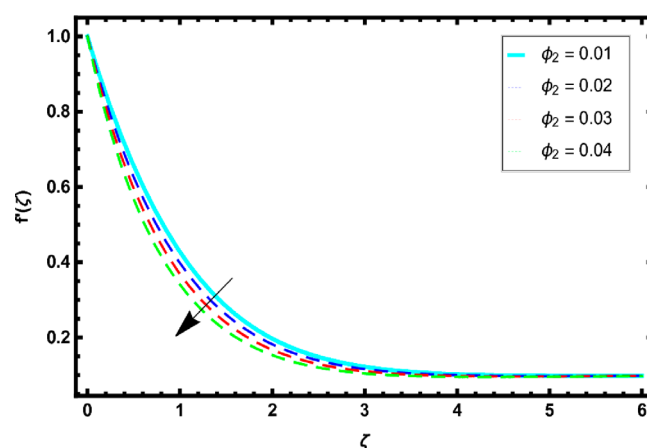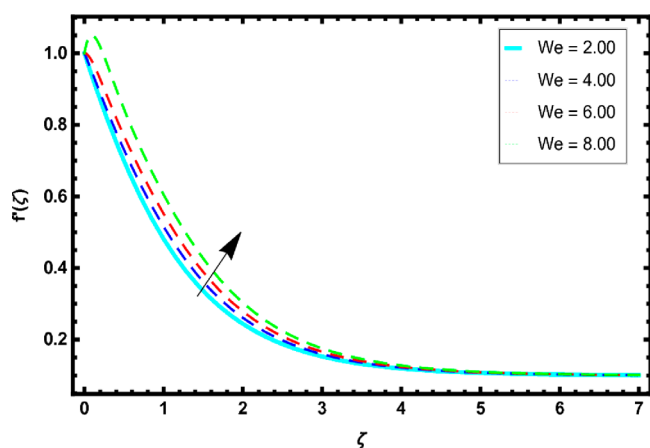


**Figure 5.** Results of velocity outline versus $\lambda$.

the greater estimates of the mixed convection parameter $\lambda$ lead to boosting the hybrid nanofluid velocity profile. The role of the power index number $n$ over the velocity profile is discussed in Figure 6. In this figure, the reduction in the hybrid nanoliquid velocity versus larger values of the power index number $n$ is examined. Figure 7 establishes the result of the buoyancy ratio constraint $Nr$ over the velocity profile. In this scrutiny, it is

**Figure 6.** Results of velocity outline versus *n*.



**Figure 9.** Results of velocity outline versus $\phi_1$.



**Figure 7.** Results of velocity outline versus *Nr*.



**Figure 10.** Results of velocity outline versus $\phi_2$.

detected that the velocity curve is raised through the higher approximation of the buoyancy ratio parameter *Nr*.

Figure 8 determines the deviation of the velocity outline with the increase of the Weissenberg number *We*. It is predicted that the velocity curve is elevated for rising values of *We*. The consequence of the nanoparticles volume fraction $\phi_1$ on the velocity field is elaborated in Figure 9. In this inquiry, it is noticed that when the nanoparticles volume fraction $\phi_1$ is higher, the velocity of the hybrid nanofluid decreases. Figure 10



**Figure 8.** Results of velocity outline versus *We*.

explores the variation of the hybrid nanofluid velocity versus escalating values of $\phi_2$. The decreasing behavior in the velocity profile is perceived to expand the estimation of the nanoparticles volume fraction $\phi_2$. The reason behind this is that when the nanomaterial quantities are enhanced then the number of the nanoparticles in the base fluid increase, which consequently diminishes the hybrid nanofluid velocity. The boundary layer thickness also increases by the mixing of the nanoparticulates in the base liquid which opposes the fluid motion.

**4.2. Microrotation profile.** The fallout of the microrotation parameter *K* and microrotation slip parameter $m_0$ on the microrotation profile of the hybrid nanoliquid is discussed in Figures 11 and 12. Figure 11 established the results of the microrotation constraint *K* on the hybrid nanoliquid microrotation profile. It is perceived that the hybrid nanoliquid microrotation profile shows decrement performance for intensifying values of the microrotation factor *K*. The significance of the microrotation slip factor $m_0$ on the microrotation profile is constructed in Figure 12. This figure explained that the expanding estimation of the microrotation slip parameter $m_0$ augmented the microrotation profile of hybrid nanofluid.

**4.3. Temperature Profile.** The roles of thermal radiation parameter *R*, *Bi*, *Ec*, thermophoresis parameter *Nt*, and heat generation parameter *Q* on the hybrid nanofluid temperature are demonstrated in Figures 13−17. Figure 13 signifies the temperature for larger values of *R*. It can be seen that the rising estimates of *R* increase the temperature. Figure 14 displays the
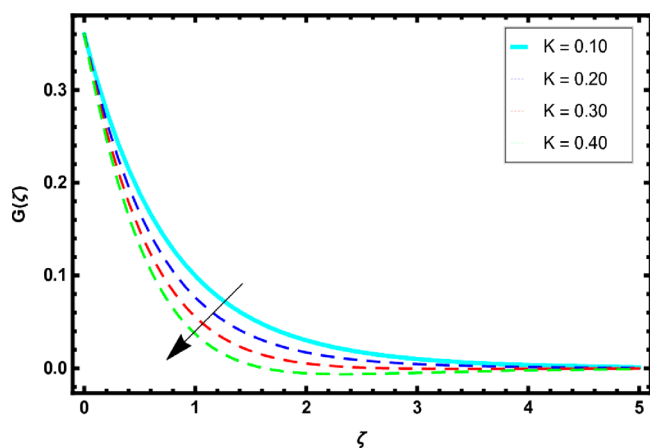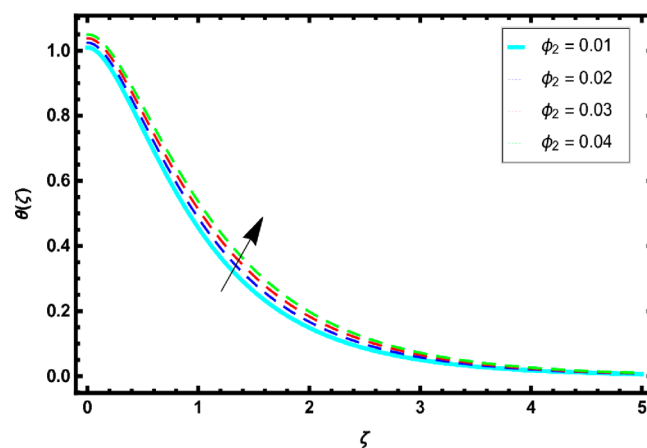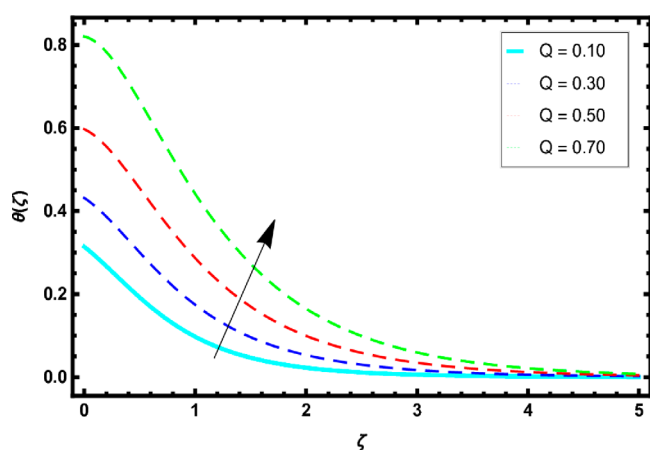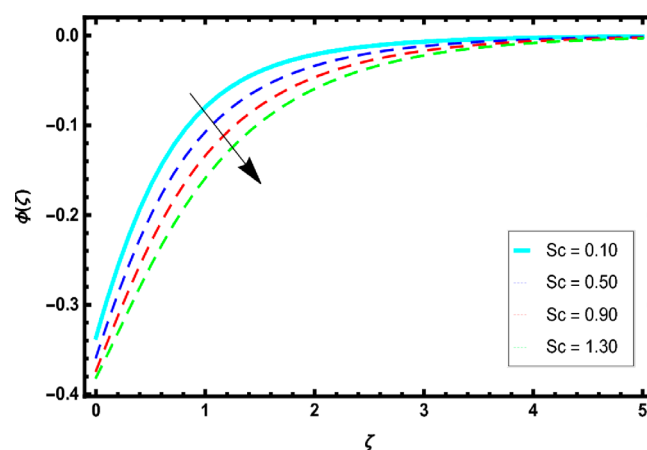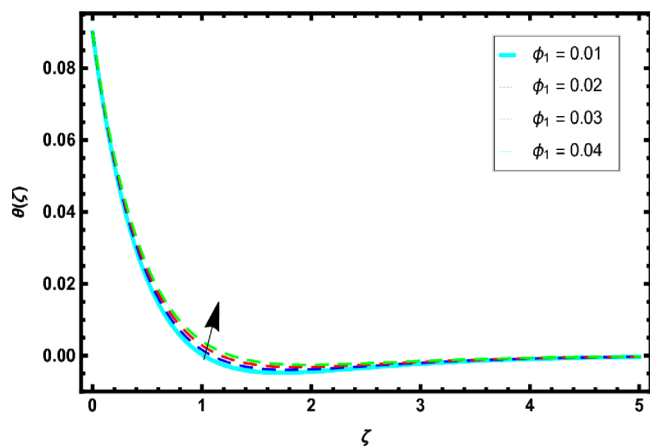
**Figure 11.** Results of hybrid nanofluid microrotation profile due to $K$.
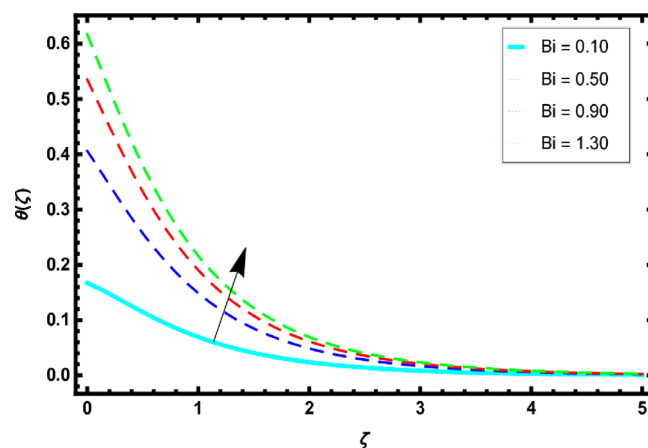


**Figure 14.** Results of energy outline versus $Bi$.
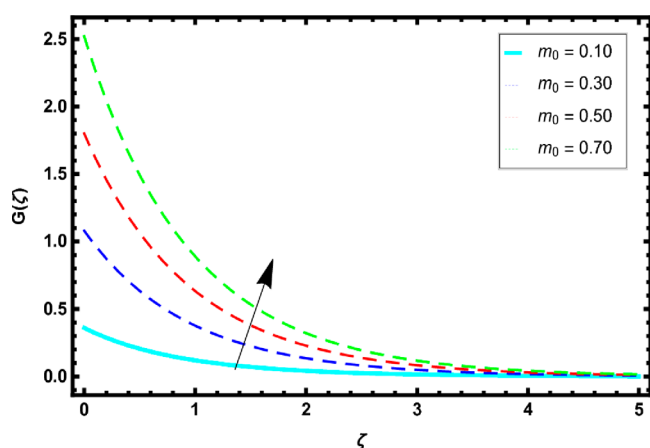


**Figure 12.** Results of hybrid nanofluid microrotation profile due to $m_0$.
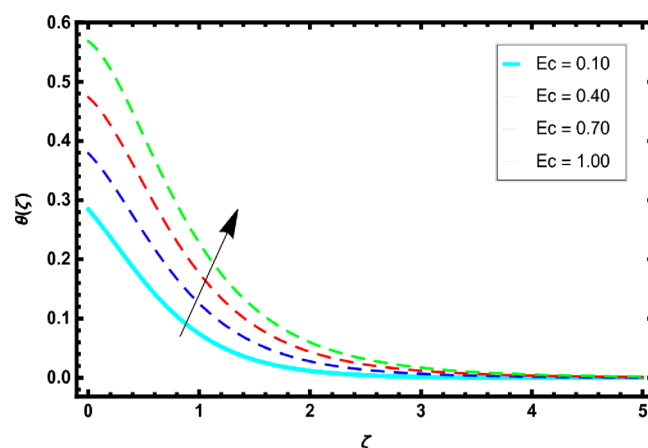


**Figure 15.** Results of energy outline versus $Ec$.
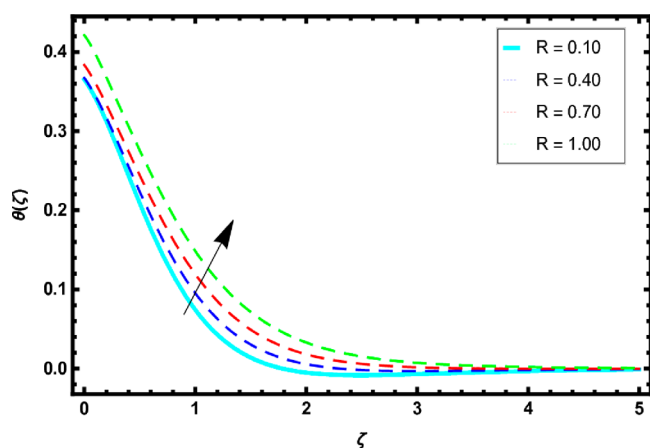


**Figure 13.** Results of energy outline versus $R$.

behavior of the energy curve under the effect of thermal Biot number $Bi$. In this figure, it is evident that the escalating values of the $Bi$ produce an increment in the hybrid nanoliquid temperature. Further, the boundary layer thickness and energy rate increase when $Bi$ rises; therefore, the hybrid nanofluid temperature profile increases. The analysis of $Ec$ on the temperature contour is displayed in Figure 15. It is depicted that the temperature increases for greater values of the Eckert number $Ec$. The drag force between the particles of the liquid is amplified due to the intensification of the Eckert number which

consequently increases the heat transport rate and alternatively the temperature of the fluid is enhanced. Further, the relationship between the kinetic energy and the heat enthalpy variation is called the Eckert number. So, the kinetic energy of the hybrid nanoliquid increases with the increase of $Ec$. The temperature is discussed as the average kinetic energy. Therefore, the hybrid nanofluid temperature rises. Figure 16 exhibits the results of the $Nt$ on the hybrid nanofluid temperature. It can be seen that the temperature declines for rising values of $Nt$.

Figure 17 is graphed to evaluate the impact of $Q$ over the temperature profile. In this analysis, it is revealed that the hybrid nanoliquid temperature is augmented for rising values of $Q$. Figure 18 is sketched for the assessment of the hybrid nanoliquid temperature with respect to the growing estimation of the nanoparticles volume fraction $\phi_1$. In this figure, it is apparent that the intensifying values of the $\phi_1$ led to an improvement of the temperature profile. The role of the nanoparticles volume fraction $\phi_2$ on the energy contour is shown in Figure 19. This figure shows that the hybrid nanoliquid temperature graph is augmented due to the augmentation of $\phi_2$. The hybrid nanofluid thermal conductivity rises when the nanoparticles are added in the base liquid. So, the thermal efficiency of the hybrid nanofluid is also enhanced, thus the temperature increases due to the increase of nanoparticles volume fraction.

**4.4. Concentration Profile.** Figures 20−22 visualize the change in the concentration of the hybrid nanoliquid via $Sc$, $Nt$,
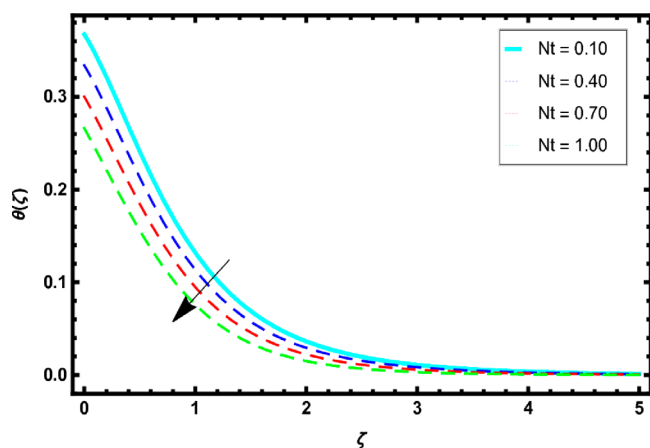
**Figure 16.** Results of energy outline versus $Nt$.



**Figure 17.** Results of energy outline versus $Q$.



**Figure 18.** Results of energy outline versus $\phi_1$.



**Figure 19.** Results of energy outline versus $\phi_2$.



**Figure 20.** Results of mass outline versus $Sc$.
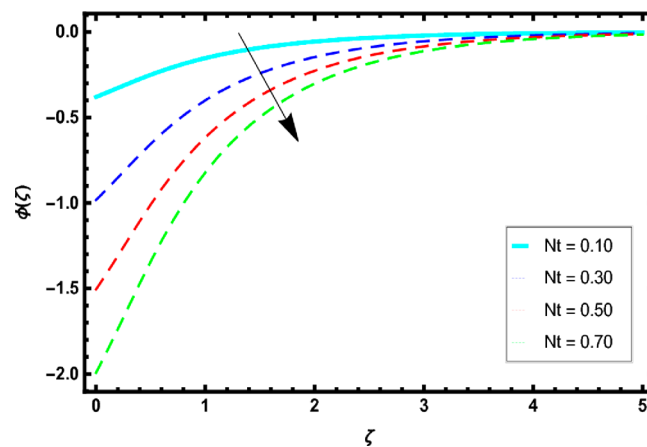


**Figure 21.** Results of mass outline versus $Nt$.

and $kr$. The physical description of the hybrid nanofluid concentration for intensifying values of $Sc$ is scrutinized in Figure 20. In this inquiry, it is eminent that the hybrid nanoliquid concentration is weakened for rising values of $Sc$. The molecular diffusivity decreases when the Schmidt number increases. So, the hybrid nanofluid concentration is enhanced with the expanding of $Sc$. Figure 21 epitomizes the impact of the $Nt$ on the mass outline. In this graph, it can be seen that the concentration field is decayed due to enhancement in the values of the $Nt$. Figure 22 addresses the results of $kr$ on the

concentration. The decline behavior in the concentration is noticed for the expanding estimation of $kr$. It is perceived that the collision between the particles of the fluid is enhanced due to the expansion of the chemical reaction parameter $kr$ near the surface which consequently reduces the concentration of the hybrid nanofluid and boundary layer thickness.

**4.5. Skin Friction and Nusselt Number.** The deviation of $C_f$ and $Nu$ versus different flow parameters in two-dimensional contour graphs are deliberated. Figure 23 examined the role of the Darcy-Forchheimer $Fr$ factor on skin friction. In this figure, it
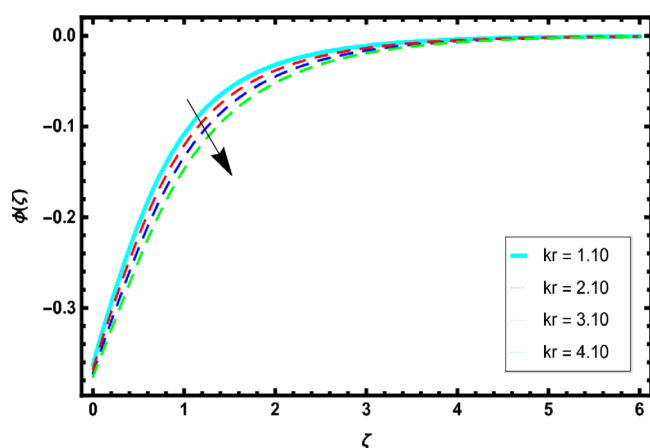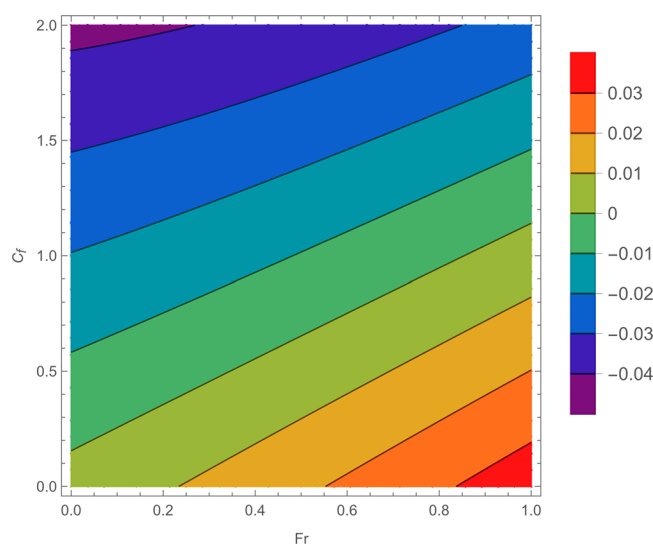
**Figure 22.** Results of mass outline versus *kr*.



**Figure 23.** 2D view of skin friction coefficient against *Fr*.

is identified that $C_f$ is decayed due to the intensifying *Fr* values. Figure 24 displayed the performance of Nusselt number *Nu* for
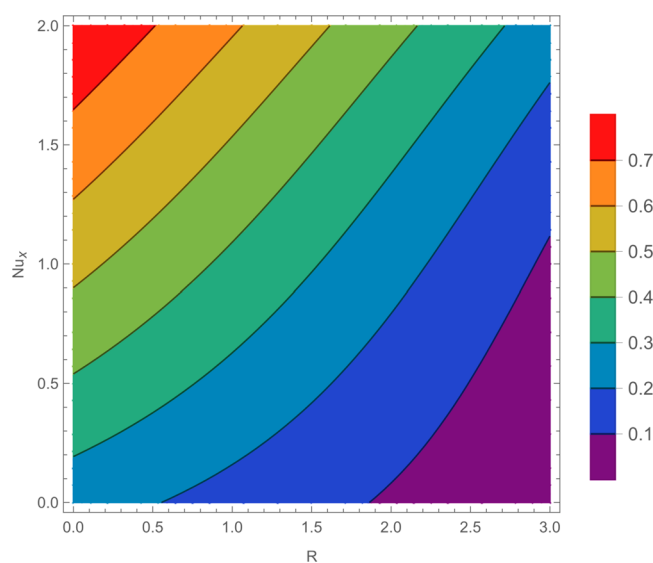


**Figure 24.** 2D view of Nusselt number against *R*.

higher values of the radiation parameter *R*. The increasing behavior in *Nu* of the hybrid nanofluid is detected for expanding values of the radiation parameter *R*.

## 5. CONCLUSION

In the current analysis, the two-dimensional mixed convection flow of *Ag*−Cu/blood-based micropolar Carreau−Yasuda fluid with Darcy-Forchheimer parameter in a porous medium by using the convectively heated Riga plate is examined. The main objective of this problem is to simulate the influence of the thermal radiation, viscous dissipation, and heat source/sink on the Ag−Cu/blood-based micropolar Carreau−Yasuda hybrid nanofluid. The phenomenon of the heat and mass transport is analyzed under the convective and partial slip conditions. The HAM technique is operated for the analytical exploration of the problem. The mathematical framework of the present problem is discussed in terms of the system of the of PDEs. With the assistance of suitable similarity transformations, these higher-order nonlinear PDEs are converted into highly nonlinear ODEs. The physical significance of the different flow parameters such as Hartmann number, Darcy-Forchheimer factor, micro-rotation, mixed convection, power index number, buoyancy ratio, Weissenberg number, microrotation slip, thermal radiation, thermal Biot number, Eckert number, thermophoresis parameter, heat generation parameter, Schmidt number, and chemical reaction on the velocity, microrotation, mass and energy profiles of the hybrid nanofluid are computed. The major concluding remarks of the present work are

- Increment performance of the hybrid nanofluid velocity is examined for Hartmann number, microrotation factor, mixed convection constraint, buoyancy ratio parameter, and Weissenberg number.
- The Darcy-Forchheimer parameter, power index number, and nanoparticle concentrations diminished the hybrid nanoliquid velocity.
- The microrotation profile of the hybrid nanoliquid increases for microrotation slip parameter but decreases for microrotation parameter.
- An enhancing behavior of the hybrid nanoliquid temperature is perceived due to the increasing radiation term, Eckert number, thermal Biot number, heat generation factor, and nanoparticle concentrations.
- The thermophoresis parameter declined the energy profile.
- The hybrid nanofluid concentration is weakened for Schmidt number and chemical reaction effect.
- It is noticed that the skin friction coefficient of the hybrid nanofluid is diminished with the escalating of the Darcy-Forchheimer parameter.
- Nusselt number of the hybrid nanofluid is higher for the radiation parameter.

**Future work.** The present problem can be extended in the future as follows:

- The present problem can be studied in the form of three-dimensional flow.
- This problem can be extended for different boundary conditions.
- This model can be extended for different base fluids such as kerosene oil, honey, engine oil, and so forth.
- In this problem the mixed convection micropolar Carreau−Yasuda hybrid nanofluid flow is analyzed, but in the future it can be studied for any non-Newtonian fluid

such as Maxwell fluid, Jeffrey fluid, Williamson fluid, or Casson fluid, etc.

- Behaviors of bioconvection, Cattaneo-Christov energy, and mass flux, entropy generation, and activation energy can be analyzed.
- For the simulation, different numerical and analytical techniques can be used.

## ■ AUTHOR INFORMATION

**Corresponding Authors**

**Anwar Saeed** − *Center of Excellence in Theoretical and Computational Science (TaCS-CoE), Science Laboratory Building, Faculty of Science, King Mongkut's University of Technology Thonburi (KMUTT), Bangkok 10140, Thailand;* ⊙ orcid.org/0000-0003-1566-6457; Email: anwarsaeed769@gmail.com

**Poom Kumam** − *KMUTT Fixed Point Research Laboratory, Room SCL 802 Fixed Point Laboratory, Science Laboratory Building, Department of Mathematics, Faculty of Science, King Mongkut's University of Technology Thonburi (KMUTT), Bangkok 10140, Thailand; Center of Excellence in Theoretical and Computational Science (TaCS-CoE), Science Laboratory Building, Faculty of Science, King Mongkut's University of Technology Thonburi (KMUTT), Bangkok 10140, Thailand; Department of Medical Research, China Medical University Hospital, China Medical University, Taichung, 40402, Taiwan;* Email: poom.kum@kmutt.ac.th

**Authors**

**Muhammad Ramzan** − *KMUTT Fixed Point Research Laboratory, Room SCL 802 Fixed Point Laboratory, Science Laboratory Building, Department of Mathematics, Faculty of Science, King Mongkut's University of Technology Thonburi (KMUTT), Bangkok 10140, Thailand; Center of Excellence in Theoretical and Computational Science (TaCS-CoE), Science Laboratory Building, Faculty of Science, King Mongkut's University of Technology Thonburi (KMUTT), Bangkok 10140, Thailand*

**Muhammad Javed** − *Centre for Advanced Studies in Pure and Applied Mathematics, Bahauddin Zakariya University, Multan, 60800, Pakistan*

**Sadique Rehman** − *Department of Pure and Applied Mathematics, University of Haripur, Haripur, Khyber Pakhtunkhwa 22620, Pakistan*

**Dawood Ahmed** − *University of Haripur, Department of Medical Laboratory Technology, Haripur, Khyber Pakhtunkhwa 22620, Pakistan*

Complete contact information is available at: https://pubs.acs.org/10.1021/acsomega.2c03570

**Notes**

The authors declare no competing financial interest.

## ■ ACKNOWLEDGMENTS

## ■ REFERENCES

(1) Abou-zeid, M. Y.; Ouaf, M. E. Hall currents effect on squeezing flow of non-Newtonian nanofluid through a porous medium between two parallel plates. *Case Studies in Thermal Engineering* **2021**, *28*, 101362.

(2) Li, Y. X.; Al-Khaled, K.; Khan, S. U.; Sun, T. C.; Khan, M. I.; Malik, M. Y. Bio-convective Darcy-Forchheimer periodically accelerated flow of non-Newtonian nanofluid with Cattaneo−Christov and Prandtl effective approach. *Case Studies in Thermal Engineering* **2021**, *26*, 101102.

(3) Imtiaz, M.; Hayat, T.; Alsaedi, A. MHD convective flow of Jeffrey fluid due to a curved stretching surface with homogeneous-heterogeneous reactions. *PLoS One* **2016**, *11* (9), e0161641.

(4) Punith Gowda, R. J.; Naveen Kumar, R.; Jyothi, A. M.; Prasannakumara, B. C.; Sarris, I. E. Impact of binary chemical reaction and activation energy on heat and mass transfer of marangoni driven boundary layer flow of a non-Newtonian nanofluid. *Processes* **2021**, *9* (4), 702.

(5) Ramzan, M.; Khan, N. S.; Kumam, P. Mechanical analysis of non-Newtonian nanofluid past a thin needle with dipole effect and entropic characteristics. *Sci. Rep.* **2021**, *11* (1), 1−25.

(6) Soomro, F. A.; Haq, R. U.; Hamid, M. Brownian motion and thermophoretic effects on non-Newtonian nanofluid flow via Crank−Nicolson scheme. *Archive of Applied Mechanics* **2021**, *91* (7), 3303−3313.

(7) Bilal, M.; Urva, Y. Analysis of non-Newtonian fluid flow over fine rotating thin needle for variable viscosity and activation energy. *Archive of Applied Mechanics* **2021**, *91* (3), 1079−1095.

(8) Prasannakumara, B. C. Numerical simulation of heat transport in Maxwell nanofluid flow over a stretching sheet considering magnetic dipole effect. *Partial Differential Equations in Applied Mathematics* **2021**, *4*, 100064.

(9) Ramzan, M.; Saeed, A.; Kumam, P.; Ahmad, Z.; Junaid, M. S.; Khan, D. Influences of Soret and Dufour numbers on mixed convective and chemically reactive Casson fluids flow towards an inclined flat plate. *Heat Transfer* **2022**, *51*, 4393.

(10) Ramzan, M.; Shah, Z.; Kumam, P.; Khan, W.; Watthayu, W.; Kumam, W. Bidirectional flow of MHD nanofluid with Hall current and Cattaneo-Christove heat flux toward the stretching surface. *PLoS One* **2022**, *17* (4), e0264208.

(11) Arif, M.; Kumam, P.; Kumam, W.; Khan, I.; Ramzan, M. A fractional model of Casson fluid with ramped wall temperature: engineering applications of engine oil. *Computational and Mathematical Methods* **2021**, *3* (6), e1162.

(12) Eswaramoorthi, S.; Divya, S.; Faisal, M.; Namgyel, N. Entropy and Heat Transfer Analysis for MHD Flow of-Water-Based Nanofluid on a Heated 3D Plate with Nonlinear Radiation. *Math. Problems Eng.* **2022**, *2022*, 1.

(13) Alshehri, A.; Shah, Z. Computational analysis of viscous dissipation and Darcy-Forchheimer porous medium on radioactive hybrid nanofluid. *Case Studies in Thermal Engineering* **2022**, *30*, 101728.

(14) Waqas, H.; Farooq, U.; Alqarni, M. S.; Muhammad, T. Numerical investigation for 3D bioconvection flow of Carreau nanofluid with heat source/sink and motile microorganisms. *Alexandria Engineering Journal* **2022**, *61* (3), 2366−2375.

(15) Muhammad, T.; Waqas, H.; Manzoor, U.; Farooq, U.; Rizvi, Z. F. On doubly stratified bioconvective transport of Jeffrey nanofluid with gyrotactic motile microorganisms. *Alexandria Engineering Journal* **2022**, *61* (2), 1571−1583.

(16) Nadeem, S.; Mehmood, R.; Motsa, S. S. Numerical investigation on MHD oblique flow of Walter's B type nano fluid over a convective surface. *International Journal of Thermal Sciences* **2015**, *92*, 162−172.

(17) Ramzan, M.; Algehyne, E. A.; Saeed, A.; Dawar, A.; Kumam, P.; Watthayu, W. Homotopic simulation for heat transport phenomenon of the Burgers nanofluids flow over a stretching cylinder with thermal convective and zero mass flux conditions. *Nanotechnol. Rev.* **2022**, *11* (1), 1437−1449.

(18) Bilal, M.; Ayed, H.; Saeed, A.; Brahmia, A.; Gul, T.; Kumam, P. The parametric computation of nonlinear convection magneto-

hydrodynamic nanofluid flow with internal heating across a fixed and spinning disk. *Waves in Random and Complex Media* **2022**, 1−16.

(19) Akbar, Y.; Iqbal, J.; Hussain, M.; Khan, H.; Alotaibi, H. Peristaltic transportation of Carreau−Yasuda magneto nanofluid embedded in a porous medium with heat and mass transfer. *Waves in Random and Complex Media* **2022**, 1−21.

(20) Li, Z.; Barnoon, P.; Toghraie, D.; Dehkordi, R. B.; Afrand, M. Mixed convection of non-Newtonian nanofluid in an H-shaped cavity with cooler and heater cylinders filled by a porous material: Two-phase approach. *Advanced Powder Technology* **2019**, *30* (11), 2666−2685.

(21) Kavusi, H.; Toghraie, D. A comprehensive study of the performance of a heat pipe by using of various nanofluids. *Advanced powder technology* **2017**, *28* (11), 3074−3084.

(22) Moraveji, A.; Toghraie, D. Computational fluid dynamics simulation of heat transfer and fluid flow characteristics in a vortex tube by considering the various parameters. *Int. J. Heat Mass Transfer* **2017**, *113*, 432−443.

(23) Ruhani, B.; Barnoon, P.; Toghraie, D. Statistical investigation for developing a new model for rheological behavior of Silica−ethylene glycol/Water hybrid Newtonian nanofluid using experimental data. *Physica A: Statistical Mechanics and Its Applications* **2019**, *525*, 616−627.

(24) Mostafazadeh, A.; Toghraie, D.; Mashayekhi, R.; Akbari, O. A. Effect of radiation on laminar natural convection of nanofluid in a vertical channel with single-and two-phase approaches. *J. Therm. Anal. Calorim.* **2019**, *138* (1), 779−794.

(25) Arasteh, H.; Mashayekhi, R.; Goodarzi, M.; Motaharpour, S. H.; Dahari, M.; Toghraie, D. Heat and fluid flow analysis of metal foam embedded in a double-layered sinusoidal heat sink under local thermal non-equilibrium condition using nanofluid. *J. Therm. Anal. Calorim.* **2019**, *138* (2), 1461−1476.

(26) Bazdar, H.; Toghraie, D.; Pourfattah, F.; Akbari, O. A.; Nguyen, H. M.; Asadi, A. Numerical investigation of turbulent flow and heat transfer of nanofluid inside a wavy microchannel with different wavelengths. *J. Therm. Anal. Calorim.* **2020**, *139* (3), 2365−2380.

(27) Mashayekhi, R.; Khodabandeh, E.; Akbari, O. A.; Toghraie, D.; Bahiraei, M.; Gholami, M. CFD analysis of thermal and hydrodynamic characteristics of hybrid nanofluid in a new designed sinusoidal double-layered microchannel heat sink. *J. Therm. Anal. Calorim.* **2018**, *134* (3), 2305−2315.

(28) Toghraie, D.; Mashayekhi, R.; Arasteh, H.; Sheykhi, S.; Niknejadi, M.; Chamkha, A. J. Two-phase investigation of water-Al2O3 nanofluid in a micro concentric annulus under non-uniform heat flux boundary conditions. *Int. J. Numer. Methods Heat Fluid Flow* **2019**, *30*, 1795.

(29) Xia, W. F.; Hafeez, M. U.; Khan, M. I.; Shah, N. A.; Chung, J. D. Entropy optimized dissipative flow of hybrid nanofluid in the presence of non-linear thermal radiation and Joule heating. *Sci. Rep.* **2021**, *11* (1), 1−16.

(30) Naveen Kumar, R.; Mallikarjuna, H. B.; Tigalappa, N.; Punith Gowda, R. J.; Umrao Sarwe, D. Carbon nanotubes suspended dusty nanofluid flow over stretching porous rotating disk with non-uniform heat source/sink. *International Journal for Computational Methods in Engineering Science and Mechanics* **2022**, *23* (2), 119−128.

(31) Jamshed, W.; Nisar, K. S.; Ibrahim, R. W.; Mukhtar, T.; Vijayakumar, V.; Ahmad, F. Computational frame work of Cattaneo-Christov heat flux effects on Engine Oil based Williamson hybrid nanofluids: A thermal case study. *Case Studies in Thermal Engineering* **2021**, *26*, 101179.

(32) Anuar, N. S.; Bachok, N. Double solutions and stability analysis of micropolar hybrid nanofluid with thermal radiation impact on unsteady stagnation point flow. *Mathematics* **2021**, *9* (3), 276.

(33) Mabood, F.; Yusuf, T. A.; Khan, W. A. Cu−Al2O3−H2O hybrid nanofluid flow with melting heat transfer, irreversibility analysis and nonlinear thermal radiation. *J. Therm. Anal. Calorim.* **2021**, *143* (2), 973−984.

(34) Punith Gowda, R. J.; Naveen Kumar, R.; Prasannakumara, B. C. Two-phase Darcy-Forchheimer flow of dusty hybrid nanofluid with

viscous dissipation over a cylinder. *International Journal of Applied and Computational Mathematics* **2021**, *7* (3), 1−18.

(35) Haider, F.; Hayat, T.; Alsaedi, A. Flow of hybrid nanofluid through Darcy-Forchheimer porous space with variable characteristics. *Alexandria Engineering Journal* **2021**, *60* (3), 3047−3056.

(36) Ramzan, M.; Dawar, A.; Saeed, A.; Kumam, P.; Watthayu, W.; Kumam, W. Heat transfer analysis of the mixed convective flow of magnetohydrodynamic hybrid nanofluid past a stretching sheet with velocity and thermal slip conditions. *PLoS One* **2021**, *16* (12), e0260854.

(37) Khan, A.; Saeed, A.; Tassaddiq, A.; Gul, T.; Mukhtar, S.; Kumam, P.; Ali, I.; Kumam, W. Bio-convective micropolar nanofluid flow over thin moving needle subject to Arrhenius activation energy, viscous dissipation and binary chemical reaction. *Case Studies in Thermal Engineering* **2021**, *25*, 100989.

(38) Reddy, M. V.; Lakshminarayana, P. Cross-diffusion and heat source effects on a three-dimensional MHD flow of Maxwell nanofluid over a stretching surface with chemical reaction. *European Physical Journal Special Topics* **2021**, *230* (5), 1371−1379.

(39) Varun Kumar, R. S.; Gunderi Dhananjaya, P.; Naveen Kumar, R.; Punith Gowda, R. J.; Prasannakumara, B. C. Modeling and theoretical investigation on Casson nanofluid flow over a curved stretching surface with the influence of magnetic field and chemical reaction. *International Journal for Computational Methods in Engineering Science and Mechanics* **2022**, *23* (1), 12−19.

(40) Gul, H.; Ramzan, M.; Chung, J. D.; Chu, Y. M.; Kadry, S. Multiple slips impact in the MHD hybrid nanofluid flow with Cattaneo−Christov heat flux and autocatalytic chemical reaction. *Sci. Rep.* **2021**, *11* (1), 1−14.

(41) Gopal, D.; Saleem, S.; Jagadha, S.; Ahmad, F.; Almatroud, A. O.; Kishan, N. Numerical analysis of higher order chemical reaction on electrically MHD nanofluid under influence of viscous dissipation. *Alexandria Engineering Journal* **2021**, *60* (1), 1861−1871.

(42) Lv, Y. P.; Shaheen, N.; Ramzan, M.; Mursaleen, M.; Nisar, K. S.; Malik, M. Y. Chemical reaction and thermal radiation impact on a nanofluid flow in a rotating channel with Hall current. *Sci. Rep.* **2021**, *11* (1), 1−17.

(43) Punith Gowda, R. J.; Naveen Kumar, R.; Jyothi, A. M.; Prasannakumara, B. C.; Sarris, I. E. Impact of binary chemical reaction and activation energy on heat and mass transfer of marangoni driven boundary layer flow of a non-Newtonian nanofluid. *Processes* **2021**, *9* (4), 702.

(44) Rasheed, H. U.; Islam, S.; Helmi, M. M.; Alsallami, S. A.; Khan, Z.; Khan, I. An analytical study of internal heating and chemical reaction effects on MHD flow of nanofluid with convective conditions. *Crystals* **2021**, *11* (12), 1523.

(45) Rehman, A.; Hussain, A.; Nadeem, S. Assisting and opposing stagnation point pseudoplastic nano liquid flow towards a flexible Riga sheet: a computational approach. *Math. Problems Eng.* **2021**, *2021*, 1.

(46) Alotaibi, H.; Rafique, K. Numerical Analysis of Micro-Rotation Effect on Nanofluid Flow for Vertical Riga Plate. *Crystals* **2021**, *11* (11), 1315.

(47) Nayak, M. K.; Shaw, S.; Makinde, O. D.; Chamkha, A. J. Investigation of partial slip and viscous dissipation effects on the radiative tangent hyperbolic nanofluid flow past a vertical permeable Riga plate with internal heating: Bungiorno model. *Journal of Nanofluids* **2019**, *8* (1), 51−62.

(48) Mohammed Alshehri, A.; Huseyin Coban, H.; Ahmad, S.; Khan, U.; Alghamdi, W. M. Buoyancy Effect on a Micropolar Fluid Flow Past a Vertical Riga Surface Comprising Water-Based SWCNT−MWCNT Hybrid Nanofluid Subject to Partially Slipped and Thermal Stratification: Cattaneo−Christov Model. *Math. Problems Eng.* **2021**, *2021*, 1.

(49) Basha, H. T.; Rajagopal, K.; Ahammad, N. A.; Sathish, S.; Gunakala, S. R. Finite Difference Computation of Au-Cu/Magneto-Bio-Hybrid Nanofluid Flow in an Inclined Uneven Stenosis Artery. *Complexity* **2022**, *2022*, 1.

(50) Algehyne, E. A.; Alharbi, A. F.; Saeed, A.; Dawar, A.; Ramzan, M.; Kumam, P. Analysis of the MHD partially ionized GO-Ag/water and

GO-Ag/kerosene oil hybrid nanofluids flow over a stretching surface with Cattaneo−Christov double diffusion model: A comparative study. *International Communications in Heat and Mass Transfer* **2022**, *136*, 106205.

(51) Ramzan, M.; Dawar, A.; Saeed, A.; Kumam, P.; Sitthithakerngkiet, K.; Lone, S. A. Analysis of the partially ionized kerosene oil-based ternary nanofluid flow over a convectively heated rotating surface. *Open Physics* **2022**, *20* (1), 507−525.

(52) Ramzan, M.; Khan, N. S.; Kumam, P.; Khan, R. A numerical study of chemical reaction in a nanofluid flow due to rotating disk in the presence of magnetic field. *Sci. Rep.* **2021**, *11* (1), 1−24.

(53) Khan, N. S.; Humphries, U. W.; Kumam, W.; Kumam, P.; Muhammad, T. Bioconvection Casson nanoliquid film sprayed on a stretching cylinder in the portfolio of homogeneous-heterogeneous chemical reactions. *ZAMM-Journal of Applied Mathematics and Mechanics/Zeitschrift für Angewandte Mathematik und Mechanik* **2022**, *102* (5), e202000222.

(54) Usman, A. H.; Khan, N. S.; Rano, S. A.; Kumam, P. Computational investigations of Arrhenius activation energy and entropy generation in a viscoelastic nanofluid flow thin film sprayed on a stretching cylinder. *Journal of Advanced Research in Fluid Mechanics and Thermal Sciences* **2021**, *86* (1), 27−51.

(55) Rehman, S.; Anjum, A.; Farooq, M.; Hashim; Malik, M.Y. Melting heat phenomenon in thermally stratified fluid reservoirs (Powell-Eyring fluid) with joule heating. *International Communications in Heat and Mass Transfer* **2022**, *137*, 106196.